Received: 5 September 2022 | Revised: 19 May 2024 | Accepted: 23 July 2024

IET Renewable Power Generation

DOI: 10.1049/rpg2.13067

The Institution of Engineering and Technology WILEY

ORIGINAL RESEARCH

Fractional order slide mode droop control for simultaneous voltage and frequency regulation of AC microgrid

Mohamad Issa Ibraheem[1] | **Mehdi Edrisi**[1] | **Hassan Haes Alhelou**[2] | **Mehdi Gholipour**[1]

[1]Department of Electrical Engineering, Faculty of Engineering, University of Isfahan, Isfahan, Iran

[2]School of Engineering, Massachusetts Institute of Technology (MIT), Cambridge, United States

Correspondence
Mehdi Edrisi, Department of Electrical Engineering, Faculty of Engineering, University of Isfahan, Isfahan, Iran.
Email: edrisi@eng.ui.ac.ir

Abstract

This research proposes the application of fractional-order sliding mode control (FOSMC) at the primary controller level to improve the stability of an islanded microgrid by adjusting its voltage and frequency. The control strategies used in the microgrid are performed in two levels (primary and secondary) in the islanded mode. Practically, most previous studies have worked to improve the primary controller. Droop control is one of the most commonly used methods at the primary level and is adopted in this study as well. The sliding mode control (SMC) strategy is normally used to control linear equations. Thus, the nonlinear microgrid equations were transformed into some linear ones using the input-output feedback linearization technique. Further, a fractional sliding surface was acquainted. The sliding surface and FOSMC were designed to reject system uncertainties and organize the voltage and frequency. Design parameters were chosen using the Lyapunov stability theorem. The validation of the proposed method using Simulink-MATLAB confirms its effectiveness in enhancing level power sharing, regulating frequency, and maintaining voltage stability across the system.

1 | INTRODUCTION

Electricity generated by the utility grid is primarily sourced from burning fossil fuels and natural gas, resulting in the release of harmful gases like CO_2. The increasing cost of fossil fuels has prompted researchers to shift towards renewable resources, maintaining power generation while addressing climate change concerns [1]. Renewable energy sources (RESs) show promise as an eco-friendly option for future energy needs in utility grids, potentially leading to their transition into microgrids [2, 3]. Microgrids initially emerged in remote regions with limited and costly power access but have since gained recognition and popularity, expanding into urban areas [4].

The smart grid relies on renewable energy sources (RES) such as solar, wind, and tidal energy. The variability of RES can cause instability in the smart grid. To address this issue, energy storage systems (ESS) like batteries or flywheels can be utilized to offset energy fluctuations. However, ESS alone may not be sufficient for consistent power generation, as changes in power load can lead to fluctuations in power flow. Therefore, a controller is essential to maintain system stability and prevent blackouts [2].

In a microgrid system, the hierarchical controller is considered the most effective solution for balancing the load and sources. The hierarchical controller consists of three levels (primary, secondary, and tertiary) in connected mode microgrids, and two levels (primary and secondary) in islanded mode microgrids. Each level serves different functions [5].

The primary controller focuses on regulating fundamental microgrid parameters, such as frequency and voltage, which can be disrupted by changes in load or source. It also offers plug-and-play capability. However, the primary controller is not able to completely correct deviations in frequency and voltage. To address these deviations and eliminate errors, the secondary controller is used. When the microgrid is connected to the utility grid, the tertiary controller is employed to manage power flow and ensure optimal system performance [6].

The techniques used in the primary controller can further be divided into two methods, (a) communication-based and (b) non-communication-based method. Each technique has advantages, disadvantages, and strategies [7]. Communication-based methods are better than non-communication-based methods in terms of power sharing and transient response, which are considered to be flexible and easy to implement. In addition, communication-based encompass the centralized control, master-slave strategy, distributed control, and angle droop control methods, while non-communication-based methods include droop control, virtual ω, U frame, and droop control with virtual output impedance loops method. The centralized control method was introduced by Shanxu et al. [8] and requires the centre control unit to calculate the total load and send the reference current and frequency to all distribute generators (DGs). The master-slave method was introduced by Caldognetto and Tenti [9] in which they considered one of the DGs as the master that provided the reference voltage and frequency to all slave DGs. Moreover, the distributed control method was introduced by Prodanovic and Green [10]. Although this method does not need the centre control unit, each DG contains a control unit to generate the reference voltage and frequency. The angle droop distributer method also falls into this category. The diagram and illustration of this method have been explained by Majumder et al. [11]. The non-communication-based method contains droop control which is the most commonly used method in the primary controller (this method's equation has been explained in some previous studies [5, 12, 13]). However, droop control has some disadvantages in dealing with non-linear load and unbalanced load which reduces the power quality. Thus, researchers seek to improve this method and enhance the performance of the system using droop control. Consequently, some previous studies [14–16] have presented some changes in the droop equation by adding a non-linear term with the goal of making the microgrid system capable of dealing with non-linear load. To enhance the dynamic performance, a derivative term is added to the droop equation. In addition, an improved mode-adaptive droop control (MADC) was presented to reduce the adversative effect of voltage drop, and enhance power sharing. MADC is proposed as an improvement on traditional droop control to enhance the reliability, litheness, and scalability of the DC microgrid [17]. The disadvantage of the droop controller that is represented by the existing inductance or resistance between the DG and inverter is corrected by a combination of distributed local control schemes along with the basic droop control. The proposed controller removes the limitations of droop control by neglecting the line resistances between geographically distributed generators [18]. Dheer et al. presented a modification of the droop control and used adaptive nominal voltage to improve the reactive power sharing when the traditional droop fails to achieve proportional reactive power sharing in the islanded microgrid. However, the proposed method does not require information about feeder impedance or to swap data between sources [19]. An algorithm is also applied in the droop controller; an improved particle swarm optimization (IPSO) algorithm is proposed to solve any local voltage deviation, which may occur as a result of the difference in line impedance in the microgrid with multiple distributed generations [20]. In another study [21], the PSO algorithm was used to determine the optimal controller parameters. Virtual impedance and dynamic droop gains are applied to the microgrid containing two parallel inverters to improve stability and transient response. Yuan et al. [22] analysed the efficiency issue using the Lagrange multiplier method to improve the operation efficiency of microgrids under different load profiles. Keyvani et al. proposed an improved method of droop control to enhance active and reactive power sharing by correcting the slop of the droop characteristics [23]. Wherein a clear signal was applied to the microgrid to detect the error in the reactive energy sharing, and then incorporating a new term in $P-\omega$ to adjust the $Q-E$ slope, in order to achieve the reactive energy sharing accuracy. Also, an improved droop control strategy that combines the virtual impedance control with the improved droop control was proposed in [24], in order to provide power sharing with f/V restoration. A model predictive control approach was presented in [25] to regulate voltage and frequency at the point of common coupling (PCC) so as to overcome the errors that occurred in conventional droop control when active and reactive power were coupled during voltage and frequency control. The parameters of the proportional integral (PI) controller were automatically modified by Dashtdar et al., using PSO and genetic algorithms (GA) to control voltage and frequency and make dynamic response stable, particularly when the microgrid is operating in island mode or when there is a load change [26].

In this study, a sliding mode control approach is proposed for the primary controller in two interconnected microgrids. The dynamic equation of the system, incorporating droop control, is employed to derive the control law. When dealing with non-linear dynamic equations, input-output feedback linearization is applied to convert them into linear equations and ensure stable zero dynamic states for overall system stability.

The key contributions of this research include:

- Converting the non-linear dynamic equations of interconnected microgrids into linear equations through input-output feedback linearization, while maintaining stability of zero dynamic states.
- Designing a control law for the system using three different sliding surface control methods and comparing their performance in terms of system responses.
- Enhancing the sharing of active and reactive power within the system.

This article is structured as follows: The electrodynamic equations of the microgrid are explored in Section 2. Section 3 delves into the transformation of these non-linear equations into linear ones, with the aim of deriving a control law. Following this, a sliding fractional surface is designed and the Lyapunov stability method is used to verify the stability of the controller in Section 4. Section 5 provides detailed descriptions of the outcomes of the proposed method using MATLAB/Simulink. The article concludes with a summary of the findings.

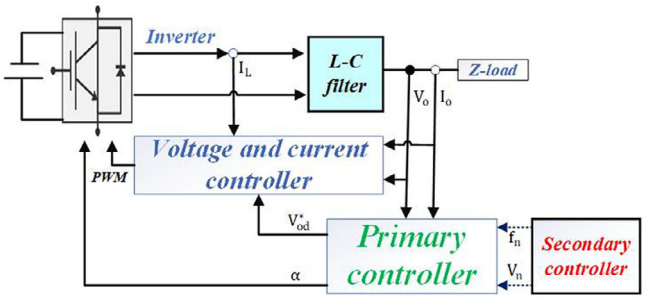

FIGURE 1 The block diagram of an inverter-based distribute generator (DG).

2 | MICROGRID NON-LINEAR EQUATIONS

Figure 1 shows a microgrid network which contains an inverter and traditional droop controller. The reference value of the frequency and voltage are generated in the secondary control, then, the droop control is used to adjust the power sharing and enhance the grid frequency and voltage.

In this block, there are two low-pass filters that filter the active and reactive power. However, the output of the primary control is the (α) angle of the DG, which represents the angle between the reference frame and reference direct output voltage (V^*_{odi}). After converting each three-phase non-linear dynamic to its own direct quadrature ($d-q$) reference frame [27], droop control Equations (1a–d) are achieved.

$$f = f_n - m_p P \tag{1a}$$

$$V^*_{od} = V_n - n_q Q \tag{1b}$$

$$V^*_{oq} = 0 \tag{1c}$$

$$\alpha = 2\pi \int f dt \tag{1d}$$

where m_p and n_q are the droop coefficients selected based on the active and reactive power ratings of the DG. f, and f_n are the system frequency and the reference frequency, respectively.

The angle of the DG is directly used in the pulse width modulation (PWM), while (V^*_{od} and V^*_{oq}) can be used to improve the primary control [28, 29]. Therefore, the non-linear dynamics of the inverter-based DG in the $d-q$ reference frame can be written as Equations (2a–i).

$$\dot{x}_1 = 2\pi\left(f_n - m_p x_2\right) \tag{2a}$$

$$\dot{x}_2 = \omega_c\left(x_6 x_8 + x_7 x_9 - x_2\right) \tag{2b}$$

$$\dot{x}_3 = \omega_c\left(x_6 x_9 - x_7 x_8 - x_3\right) \tag{2c}$$

$$\dot{x}_4 = -\frac{R_f}{L_f}x_4 + \omega_{com} x_5 + \frac{V_n - n_q x_3 - x_6}{L_f} \tag{2d}$$

$$\dot{x}_5 = -\frac{R_f}{L_f}x_5 - \omega_{com} x_4 - \frac{x_7}{L_f} \tag{2e}$$

$$\dot{x}_6 = \omega_{com} x_7 + \frac{x_4 - x_8}{C_f} \tag{2f}$$

$$\dot{x}_7 = -\omega_{com} x_6 + \frac{x_5 - x_9}{C_f} \tag{2g}$$

$$\dot{x}_8 = -\frac{R_l}{L_l}x_8 + \omega_{com} x_9 + \frac{x_6 - V_d}{L_l} \tag{2h}$$

$$\dot{x}_9 = -\frac{R_l}{L_l}x_9 - \omega_{com} x_8 + \frac{x_7 - V_q}{L_l} \tag{2i}$$

where $x_i = [\alpha\ P\ Q\ I_{Ld}\ I_{Lq}\ V_{od}\ V_{oq}\ I_{od}\ I_{oq}]$, ω_c is the cut-off frequency of the low-pass filter used in the primary control to filter active and reactive powers, V_{od} is the direct output voltage, V_{oq} is the quadrature output voltage, I_{od} is the direct output current, I_{oq} is the quadrature output current, R_l and L_l are the line resistor and inductor, respectively, R_f, L_f, and C_f are the filter resistor, inductor, and capacitor, respectively, and ω_{com} is the frequency of the common reference frame.

The system presented by Equation (2) is a multi-input multi-output (MIMO) system, where V^*_{od} and V_q are considered as the inputs (u_1, u_2) of the systems, and V_{od} and V_{oq} state variables are considered as the outputs of the system. However, the system given in Equation (2) has nine state variables. As can be seen in Equation (2), the first state variable x_1, which is α, has no effect on the other state variables, but the second state variable (P) has effect on the first variable (α). Therefore, the first state variable x_1 can be eliminated in this strategy, and the angle is directly sent to the PWM, as in some other published studies [28, 30], but the remaining states of the system will be used in the FOSMC to enhance the droop control. This means the first state in Equations (2) is deleted in this method, and the number of the state variables are reduced to the following eight states as in Equations (3a–h).

$$\dot{x}_1 = \omega_c\left(x_5 x_7 + x_6 x_8 - x_1\right) \tag{3a}$$

$$\dot{x}_2 = \omega_c\left(x_5 x_8 - x_6 x_7 - x_2\right) \tag{3b}$$

$$\dot{x}_3 = -\frac{R_f}{L_f}x_3 + \omega_{com} x_4 + \frac{u_1 - x_5}{L_f} \tag{3c}$$

$$\dot{x}_4 = -\frac{R_f}{L_f}x_4 - \omega_{com} x_3 - \frac{x_6}{L_f} \tag{3d}$$

$$\dot{x}_5 = \omega_{com} x_6 + \frac{x_3 - x_7}{C_f} \tag{3e}$$

$$\dot{x}_6 = -\omega_{com} x_5 + \frac{x_4 - x_8}{C_f} \tag{3f}$$

$$\dot{x}_7 = -\frac{R_l}{L_l}x_7 + \omega_{com} x_8 + \frac{x_5 - V_d}{L_l} \tag{3g}$$

$$\dot{x}_8 = -\frac{R_l}{L_l}x_8 - \omega_{com} x_7 + \frac{x_6 - u_2}{L_l} \tag{3h}$$

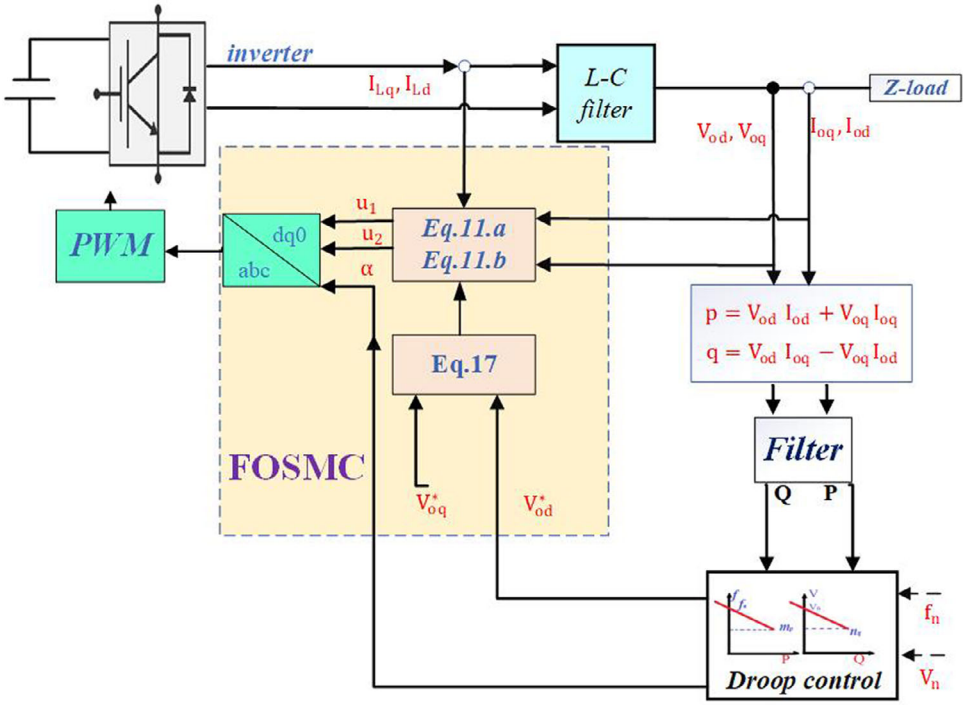

FIGURE 2 Conventional droop control system with proposed fractional-order sliding mode control (FOSMC).

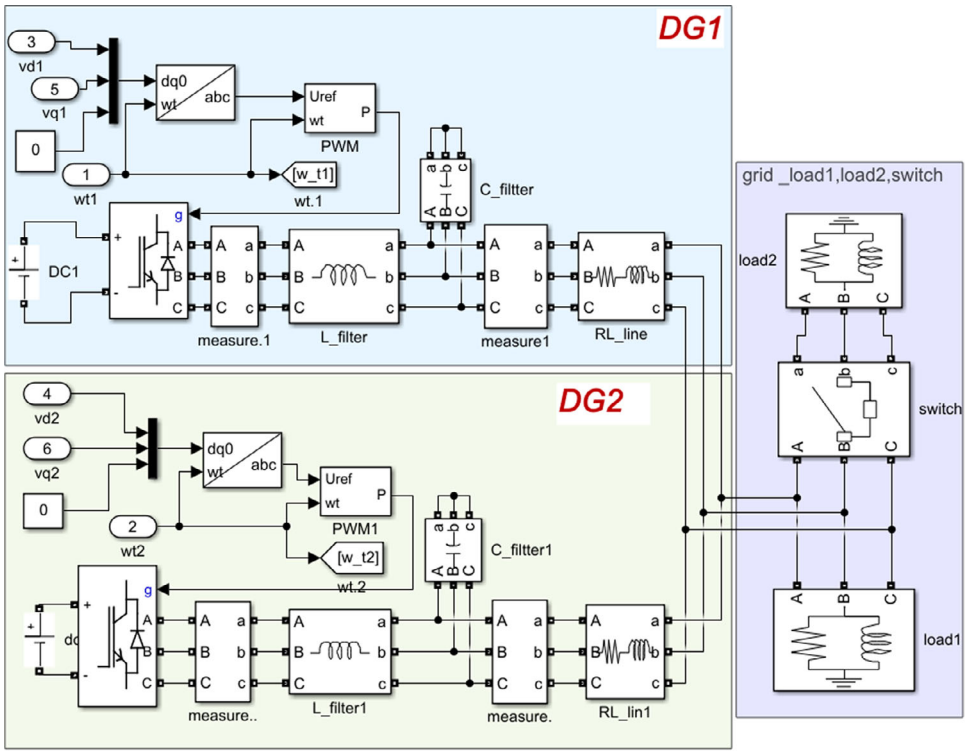

FIGURE 3 Block diagram of distribute generators (DGs) Simulink.

where x_i denotes the ith system state, and the state variable is defined as $x = [P, Q, L_d, L_q, V_{od}, V_{oq}, I_{od}, I_{oq}]$. Figure 2 shows the block diagram of the proposed strategy, where active and reactive powers are calculated and subsequently passed through a low-pass filter.

The primary controller given by Equations (1a–d) is applied to generate the reference frequency for the PWM and V^*_{od} as input to the FOSMC. Figure 3 shows the simulated block diagram model of the DGs with loads, where the PWM block provides the square pulsed wave to the inverter. Each DG

model contains an inverter, one L-C filter to achieve a sine wave, and R-L line. Model loads are associated with the DGs.

Using a linear state equation with the assumption that the used filter is an LC filter ($R_f = 0$), system Equation (3) can be rewritten as the following vector field.

$$\dot{x} = F(x) + G(x)\begin{bmatrix} u_1 \\ u_2 \end{bmatrix} \tag{4a}$$

$$Y = H(x) \tag{4b}$$

where $F(x) \in R^n$, $G(x) \in R^m$, and $H(x) \in R^p$ are the state variable, and input and output vector of the system.

$$F(x) = \begin{bmatrix} \omega_c (x_5 x_7 + x_6 x_8 - x_1) \\ \omega_c (x_5 x_8 - x_6 x_7 - x_2) \\ +\omega_{com} x_4 - \frac{x_5}{L_f} \\ -\omega_{com} x_3 - \frac{x_6}{L_f} \\ \omega_{com} x_6 + \frac{x_3 - x_7}{C_f} \\ -\omega_{com} x_5 + \frac{x_4 - x_8}{C_f} \\ -\frac{R_l}{L_l} x_7 + \omega_{com} x_8 + \frac{x_5 - V_d}{L_l} \\ -\frac{R_l}{L_l} x_8 - \omega_{com} x_7 + \frac{x_6}{L_l} \end{bmatrix}, \; G(x) = \begin{bmatrix} 0 & 0 \\ 0 & 0 \\ \frac{1}{L_f} & 0 \\ 0 & 0 \\ 0 & 0 \\ 0 & 0 \\ 0 & 0 \\ 0 & -\frac{1}{L_l} \end{bmatrix},$$

$$H(x) = [x_5; x_6] \tag{5}$$

3 | FEEDBACK LINEARIZATION

Feedback linearization is one of the control techniques, and it is used to convert non-linear system equations into linear equations. There are two feedback linearization methods, the input-output feedback linearization technique and the state-space linearization technique. To linearize using this method, the derivatives of the system's output equation are calculated repeatedly until the input appears in the resulting equation. Then, the control law is derived. The strategy used in this article is the input-output feedback technique, in which the non-linear Equations (4a,b) are converted into linear equations and the control law is formed.

Before determining the control law, the relative degree of the system should be identified and calculated. Thus, the definition of the mathematical Lie derivative is required.

Definition. Let $h(x) : R^n \to R$ be a smooth scalar function and $F(x) : R^n \to R^n$ be a smooth scaler vector field on R^n, then the Lie derivative of H with respect to F is a scaler function defined by $L_F H = \nabla H F$. Moreover, ∇H is the gradient of scalar H and is represented as:

$$\nabla H = \begin{bmatrix} \frac{\partial H}{\partial x_1} & \frac{\partial H}{\partial x_2} & .... \frac{\partial H}{\partial x_n} \end{bmatrix}$$

Thus, the Lie derivative $L_F H$ is simply the directional derivative of H along the direction of vector F [31]. Repeated Lie derivative can be defined recursively:

$$L_{F^0} H = H$$

$$L_{F^i} H = L_F (L_{F^{i-1}} H) = \nabla (L_{F^{i-1}} H) F$$

The relative degree of the MIMO system with (m) input is defined as $r = \{r_1 + r_2 + \cdots + r_m\}$, in which the following conditions are held.

1. $L_{G_i} L_F^{ri-1} H_j(x) = 0$ for $i = 1, 2 \ldots m$ and $j = 1, 2, \ldots m$
2. The $m \times m$ matrix is not singular.

$$B(x) = \begin{bmatrix} L_{G_1} L_F^{r1-1} H_1(x) & \ldots & L_{G_m} L_F^{r1-1} H_1(x) \\ L_{G_1} L_F^{r2-1} H_2(x) & \ldots & L_{G_m} L_F^{r2-1} H_2(x) \\ \vdots & \ddots & \vdots \\ \vdots & \ddots & \vdots \\ L_{G_1} L_F^{rm-1} H_m(x) & \ldots & L_{G_m} L_F^{rm-1} H_m(x) \end{bmatrix}$$

Therefore, if the relative degree is equal to the number of variables of the system, the non-linear equation can be translated into a linear equation without a zero dynamic equation. However, when the relative degree is less than the number of variables in the system, the linearization system equation can be translated as follows:

$$\begin{aligned}
&\dot{\vartheta}_1(x) = \vartheta_2(x) = L_f h_1(x) \\
&\dot{\vartheta}_2(x) = \vartheta_3(x) = L_{f^2} h_1(x) \\
&\vdots \\
&\dot{\vartheta}_{r1-1}(x) = \vartheta_{r1}(x) = L_f^{r1-1} h_1(x) \\
&\dot{\vartheta}_{r1}(x) = L_f^{r1} h_1(x) + L_{g_1} L_f^{r1-1} h_1(x) \; . u_1 + L_{g_2} L_f^{r1-1} h_1(x) \; . u_2 \\
&\dot{\psi}_1(x) = \psi_2(x) = L_f h_2(x) \\
&\dot{\psi}_2(x) = \psi_3(x) = L_{f^2} h_2(x) \\
&\vdots \\
&\dot{\psi}_{r2-1}(x) = \psi_{r2}(x) = L_f^{r2-1} h_2(x) \\
&\dot{\psi}_{r2}(x) = L_f^{r2} h_2(x) + L_{g_1} L_f^{r1-1} h_1(x) \; . u_1 + L_{g_2} L_f^{r1-1} h_2(x) \; . u_2 \\
&\dot{\eta}_1 = L_f \eta_1(x) + L_{g1} \eta_1(x) \; . u_1 + L_{g2} \eta_1(x) \; . u_2 \\
&\vdots \\
&\dot{\eta}_{n-r} = L_f \eta_{n-r}(x) + L_{g1} \eta_{n-r}(x) \; . u_1 + L_{g2} \eta_{n-r1}(x) \; . u_2
\end{aligned} \tag{6}$$

The last $(n - r)$ coordinates should be chosen such that the Jacobian matrix of the vector function $\Phi(x) = [\vartheta_1(x), \vartheta_2(x), \ldots, \vartheta_{r1}(x), \psi_1, \psi_2, \ldots, \psi_{r2}, \eta_1, \eta_2, \ldots, \eta_{n-r}]^T$ is non-singular. In addition, the field vector $\{g_1(x), g_2(x)\}$ shown in Equation (5) is not dependent on the state variable and all its elements are constant [32]. Therefore, the coordinates mapping is calculated such that:

$$L_{G_i} \eta_j = 0 \quad \text{for } i = 1, 2, 3, \ldots m \text{ and } j = 1, 2, \ldots\ldots, n - r \tag{7}$$

The previous definition is applied to the system given in Equation (5). Subsequently, matrix $B(x)$ is non-singular when $r_1 = r_2 = 2$, which means that the relative degree of the system is $r = r_1 + r_2 = 4$. According to Equation (5), the number of system variables ($n = 8$) is more than the relative degree; thus, by solving differential Equation (7) for ($m = 2$, and $j = 4$). Further, the zero dynamic states of the whole system can be chosen as $\eta_1 = x_1, \eta_2 = x_2, \eta_3 = x_7$, and $\eta_4 = x_8$. Thus, the given system in Equation (3) will be transformed into a system defined by Equation (8):

$$\dot{\vartheta}_1 = \vartheta_2 = L_F h_1(x) = \omega_{com} x_6 + \frac{x_3 - x_7}{C_f} \tag{8a}$$

$$\dot{\vartheta}_2 = L_F^2 h_1(x) + L_{g_1} L_F^1 h_1(x).u1 + L_{g_2} L_F^1 h_1(x) \tag{8b}$$

$$\dot{\psi}_1 = \psi_2 = L_F h_2(x) = -\omega_{com} x_5 + \frac{x_4 - x_8}{C_f} \tag{8c}$$

$$\dot{\psi}_2 = L_F^2 h_2(x) + L_g L_F^1 h_2(x)\, u1 + L_{g_2} L_F^1 h_2(x)\, u2 \tag{8d}$$

$$\dot{\eta}_1 = L_F \eta_1 = \omega_c (x_5 x_7 + x_6 x_8 - x_1) \tag{8e}$$

$$\dot{\eta}_2 = L_F \eta_2 = \omega_c (x_5 x_8 - x_6 x_7 - x_2) \tag{8f}$$

$$\dot{\eta}_3 = L_F \eta_3 = -\frac{R_l}{L_l}.x_7 + \omega_{com} x_8 + \frac{x_5 - V_d}{L_l} \tag{8g}$$

$$\dot{\eta}_4 = L_F \eta_4 = -\frac{R_l}{L_l} x_8 - \omega_{com} x_7 + \frac{x_6}{L_l} \tag{8h}$$

The output is the following:

$$Y_1(t) = \vartheta_1(x(t))$$

$$Y_2(t) = \psi_1(x(t))$$

And $\Phi(x)$ matrix is calculated as:

$$\Phi(x) = \begin{bmatrix} 0 & 0 & 0 & 0 & 1 & 0 & 0 & 0 \\ 0 & 0 & \frac{1}{C_f} & 0 & 0 & \omega_{\text{com}} & -\frac{1}{C_f} & 0 \\ 0 & 0 & 0 & 0 & 0 & 1 & 0 & 0 \\ 0 & 0 & 0 & \frac{1}{C_f} & -\omega_{\text{com}} & 0 & 0 & -\frac{1}{C_f} \\ 1 & 0 & 0 & 0 & 0 & 0 & 0 & 0 \\ 0 & 1 & 0 & 0 & 0 & 0 & 0 & 0 \\ 0 & 0 & 0 & 0 & 0 & 0 & 1 & 0 \\ 0 & 0 & 0 & 0 & 0 & 0 & 0 & 1 \end{bmatrix}$$

for which its determinant $\Phi(x) = -\frac{1}{C_f^2}$ is non-singular.

Consequently, $(n - r)$ equations are not controllable, and entails a subsystem called zero dynamic. These dynamics should be stable in order to guarantee the stability of the whole system. Therefore, analysing the zero dynamic equation is performed by defining:

$$h_1(x) = h_2(x) = \ldots = L_f^{r1-1} h_1(x) = L_f^{r2-1} h_2(x) = 0$$

As a result:

$$\dot{\eta}_1 = L_F \eta_1 = -x_1 \omega_c = -\omega_c \eta_1$$

$$\dot{\eta}_2 = L_F \eta_2 = -x_2 \omega_c = -\omega_c \eta_2$$

$$\dot{\eta}_3 = L_F \eta_3 = -\frac{R_l}{L_l} x_7 + \omega_{com} x_8 + \frac{-V_d}{L_l} = -\frac{R_l}{L_l} \eta_3 + \omega_{com} \eta_4 - \frac{V_d}{L_l}$$

$$\dot{\eta}_4 = L_F \eta_4 = -\frac{R_l}{L_l} x_8 - \omega_{com} x_7 = -\frac{R_l}{L_l} \eta_4 - \omega_{com} \eta_3$$

By rewriting the zero dynamic equation in the state space form as following:

$$\begin{bmatrix} \dot{\eta}_1 \\ \dot{\eta}_2 \\ \dot{\eta}_3 \\ \dot{\eta}_4 \end{bmatrix} = \begin{bmatrix} -\omega_c & 0 & 0 & 0 \\ 0 & -\omega_c & 0 & 0 \\ 0 & 0 & -\frac{R_l}{L_l} & \omega_{com} \\ 0 & 0 & -\omega_{com} & -\frac{R_l}{L_l} \end{bmatrix} \begin{bmatrix} \eta_1 \\ \eta_2 \\ \eta_3 \\ \eta_4 \end{bmatrix} + \begin{bmatrix} 0 \\ 0 \\ -\frac{V_d}{L_l} \\ 0 \end{bmatrix}$$

The eigenvalues of the zero dynamic subsystem are as follows:

$$\lambda_{1,2} = -\omega_c$$

$$\lambda_{3,4} = -\frac{R_l}{L_l} \pm \omega_{com} i$$

Now, by the consideration of V_d as a limited value in the system, the zero dynamic system is stable. However, the next step is finding the control law which makes Equation (8) into a linear equation, so the state space of Equation (8) can be written as Equation (9).

$$\begin{bmatrix} \ddot{h}_1 \\ \ddot{h}_2 \end{bmatrix} = \begin{bmatrix} L_F^2 h_1(x) \\ L_F^2 h_2(x) \end{bmatrix} + \begin{bmatrix} L_{g_1} L_F^1 h_1(x) & L_{g_2} L_F^1 h_1(x) \\ L_{g_1} L_F^1 h_2(x) & L_{g_2} L_F^1 h_2(x) \end{bmatrix} \begin{bmatrix} u_1 \\ u_2 \end{bmatrix} = \begin{bmatrix} v_1 + d_1(x) \\ v_2 + d_2(x) \end{bmatrix} \tag{9}$$

where $v = [v_1 v_2]^T$ is the auxiliary input and $d(x) = [d_1(x)\ d_2(x)]^T$ is the uncertainty in the system. Therefore, according to Equation (9), the control law which makes the equation system linear is obtained as the following:

$$\begin{bmatrix} u_1 \\ u_2 \end{bmatrix} = inv\left(\begin{bmatrix} L_{g_1} L_F h_1 & L_{g_2} L_F h_1 \\ L_{g_1} L_F h_2 & L_{g_2} L_F h_2 \end{bmatrix} \right) \times \left(- \begin{bmatrix} L_F^{r1} h_1 \\ L_F^{r2} h_2 \end{bmatrix} + \begin{bmatrix} v_1 \\ v_2 \end{bmatrix} \right) \tag{10}$$

where $\begin{bmatrix} L_{g_1} L_F h_1 & L_{g_2} L_F h_1 \\ L_{g_1} L_F h_2 & L_{g_2} L_F h_2 \end{bmatrix} = \begin{bmatrix} \frac{1}{C_f L_f} & 0 \\ 0 & \frac{1}{C_f L_l} \end{bmatrix}$

$$\begin{bmatrix} L_F^2 h_1 \\ L_F^2 h_2 \end{bmatrix} = \begin{bmatrix} 2\frac{\omega_{com}}{C_f}(x_4 - x_8) - w_{com}^2 x_5 - x_5\left(\frac{1}{L_f C_f} + \frac{1}{L_l C_f}\right) + \frac{R_l}{C_f L_l}x_7 + \frac{V_d}{L_l C_f} \\ -x_6\left(\frac{1}{C_f L_l} + \frac{1}{C_f L_f}\right) - w_{com}^2 x_6 + 2\frac{\omega_{com}}{C_f}(x_7 - x_3) + \frac{R_l}{C_f L_l}x_8 \end{bmatrix}$$

Consequently, the control law for the whole system becomes as Equation (11).

$$\begin{aligned} u_1 = {} & x_5\left(C_f L_l + C_f L_f\right) + L_l C_f^2 L_f w_{com}^2 x_5 \\ & - 2w_{com} L_l C_f L_f (x_4 - x_8) - C_f L_f R_l x_7 - C_f L_f V_d \\ & + L_l C_f^2 L_f v_1 \end{aligned} \tag{11a}$$

$$\begin{aligned} u_2 = {} & x_6\left(C_f L_l + C_f L_f\right) + L_l C_f^2 L_f w_{com}^2 x_6 \\ & - 2w_{com} L_l C_f L_f (x_7 - x_3) - C_f L_f R_l x_8 \\ & + L_l C_f^2 L_f v_2 \end{aligned} \tag{11b}$$

3.1 | Sliding surface design

Sliding surface technique is used to guarantee the transformation of the system state into a stable state and its maintenance [33]. The traditional sliding surface is known from the general law introduced by Equation (12).

$$\sigma = \left(\frac{d}{dt} + \lambda\right)^{r_i - 1} h_i \tag{12}$$

Based on the conventional sliding surface mode control, the fraction is designed using a fractional control item, which is employed as one of the integrated controls to achieve robustness. Then, the closed-loop system can reject system uncertainties, and the control input chattering is reduced. In a previous study [34], the fractional surface was defined for the model of a car and a two-link rigid robot manipulator as Equation (13).

$$\sigma = \left(\frac{d}{dt} + \lambda_1\right)^{r_i - 1} h_i - D^{\xi} h_i \tag{13}$$

where $D^{\xi} h_i$ is a fractional derivative of h_i. In this study, by considering the previous sliding surface shown in Equation (13) is used for the microgrid system, a new fraction order sliding surface is introduced to enhance the response system and reduce chattering as presented in Equation (14).

$$\sigma = \left(\frac{d}{dt} + \lambda_{i1} \int dt\right)^{ri - 1} h_i - \lambda_{i2} D^{\xi} h_i \tag{14}$$

The difference between the new design and the conventional one is an added fractional term. This term will make the system more responsive and robust. However, to find the non-linear law, let the derivative of the fraction sliding surface be defined as Equation (15):

$$\dot{\sigma} = h_i^{(r_i)} + \lambda_{i1} h_i - \lambda_{i2} D^{\xi + 1} h_i \tag{15}$$

Combining Equation (9) with Equation (15) we get:

$$\dot{\sigma} = \lambda_{i1} h_i - \lambda_{i2} D^{\xi + 1} h_i + v_i + d_i(x) \tag{16}$$

Let $\dot{\sigma} = 0$, the non-linear controller is obtained as Equation (17).

$$v_i = -\lambda_{i1} h_i + \lambda_{i2} D^{\xi + 1} h_i - K_i sign(\sigma) \tag{17}$$

where K_i is a switching feedback control gain and might be any positive number. In Equation (17), the first-order SMC item, $K_i sign(\sigma)$ (with $K_i > |d_i(x)|$) is considered as the equivalent control part to reject the system uncertainty. Moreover, $sign(.)$ is a sign function defined as Equation (18).

$$sign(\sigma) = \begin{cases} -1 & \sigma < 0 \\ 0 & \sigma = 0 \\ 1 & \sigma > 0 \end{cases} \tag{18}$$

3.2 | Lyapunov stability analysis

Lyapunov's direct method (also called the second method of Lyapunov) will be used to prove that the designed non-linear controller is stable. The Lyapunov method allows us to determine the stability of the whole system without explicitly solving the differential equations, and it is a common approach to deal with the stability problem of linear/non-linear systems [34]. The method is a generalization of the idea that if there is some "measure of energy" in a system, then one can study the rate of variation in the energy of the system to ascertain stability. To make this precise, it is necessary to define exactly what one means by a "measure of energy" or the Lyapunov function which must achieve these conditions:

1. The Lyapunov function must be positive definite function $V(x, t) \in R^+$
2. $V(0, t) = 0$

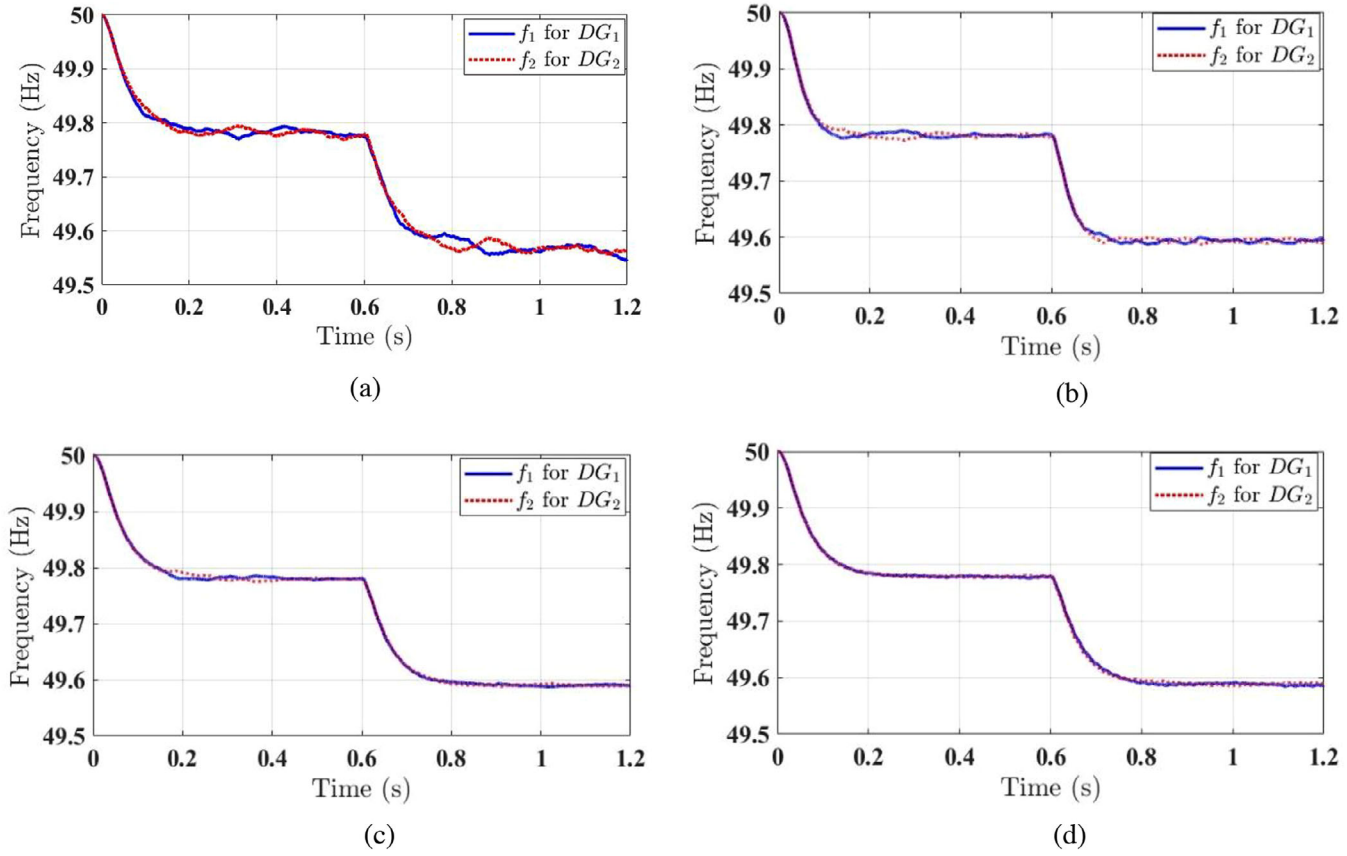

FIGURE 4 Comparing the frequency response of the system using different controllers: (a) PID, (b) Equation (12), (c) Equation (13), and (d) Equation (14).

3. Now, if $\dot{V}(x,t) < 0$, then the stability of the equilibrium point can be concluded.

Stability: Choosing the Lyapunov function as:

$$V = |\sigma| > 0$$

which is positive definite

Differentiating the Lyapunov function V we get:

$$\dot{V} = \dot{\sigma} sign(\sigma) \tag{19}$$

Combining (17) with (19) we get:

$$\dot{V} = \left(\lambda_{i1} h_i - \lambda_{i2} D^{\xi+1} h_i + h_i^{(r_i)}\right) sign(\sigma) \tag{20}$$

Substituting (9) and (11) in (20) results in:

$$\dot{V} = \left(\lambda_{i1} h_i - \lambda_{i2} D^{\xi+1} h_i + v_i\right) sign(\sigma) \tag{21}$$

Substituting (17) into (20), with respect to $K_i > |d_i(x)|$, Equation (22) will be acquired as:

$$\dot{V} = -K_i sign(\sigma)^2 \tag{22}$$

Therefore, on the basis of the Lyapunov stability theorem, the state variables of the closed-loop control system will converge to the equilibrium point if the constant variable K_i is chosen positive and greater than $|d_i(x)|$. That means the non-linear controller can stabilize the whole system.

TABLE 1 Model and controller parameters.

Model parameters		Controller parameters	
DC voltage	470 V	ω_c	20 Hz
Frequency	50 Hz	m_p, n_q	$0.7\,e-4,\ 1\,e-4$
Line voltage	$220\sqrt{3}$ V	$\frac{Q_1}{Q_2} = \frac{n_{q2}}{n_{q1}}$, $\frac{P_1}{P_2} = \frac{m_{p2}}{m_{p1}}$	1
Inductance filter	10 mH	K_i	$1\,e13$
Capacitance filter	100 μF	$\lambda_{11}, \lambda_{12}$	$1\,e10, 6\,e3$
Resistance line DG_1, DG_2	1.346, 1.2Ω	$\lambda_{21} = \lambda_{22}$	100
Inductance line DG_1, DG_2	0.6, 0.5 mH	ξ	0.5

4 | SIMULATION STUDY

Simulink/MATLAB is used to build the microgrid model. The proposed model contains two parallel inverters connected to the two loads. The first load is (6 kW + 1.5 kVar), and the second load is similar to the first load in terms of capacity and is connected to the grid at time ($t = 0.6$ s). The model and controller parameters are present in Table 1.

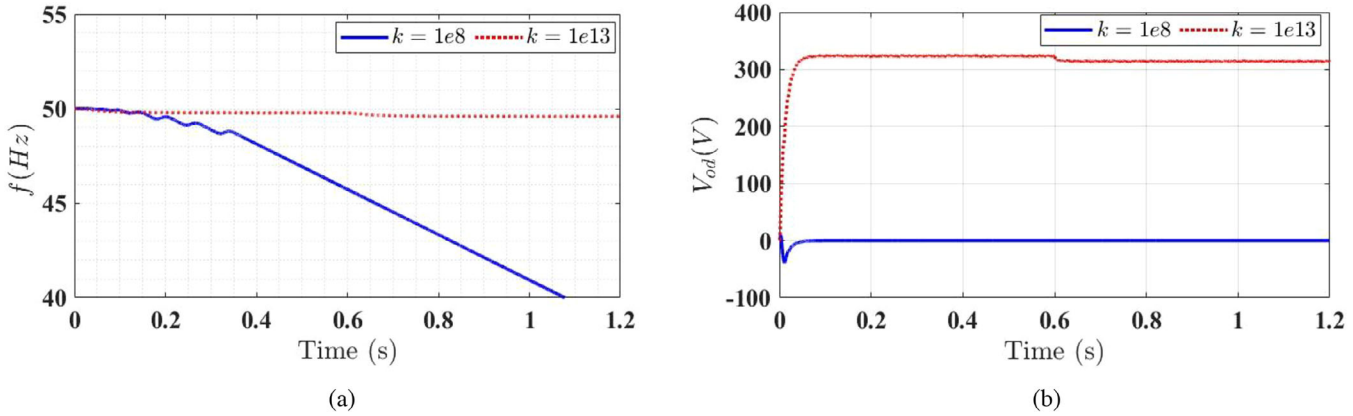

FIGURE 5 Effect of changing the switch gain parameter of the system: (a) frequency, (b) direct output voltage.

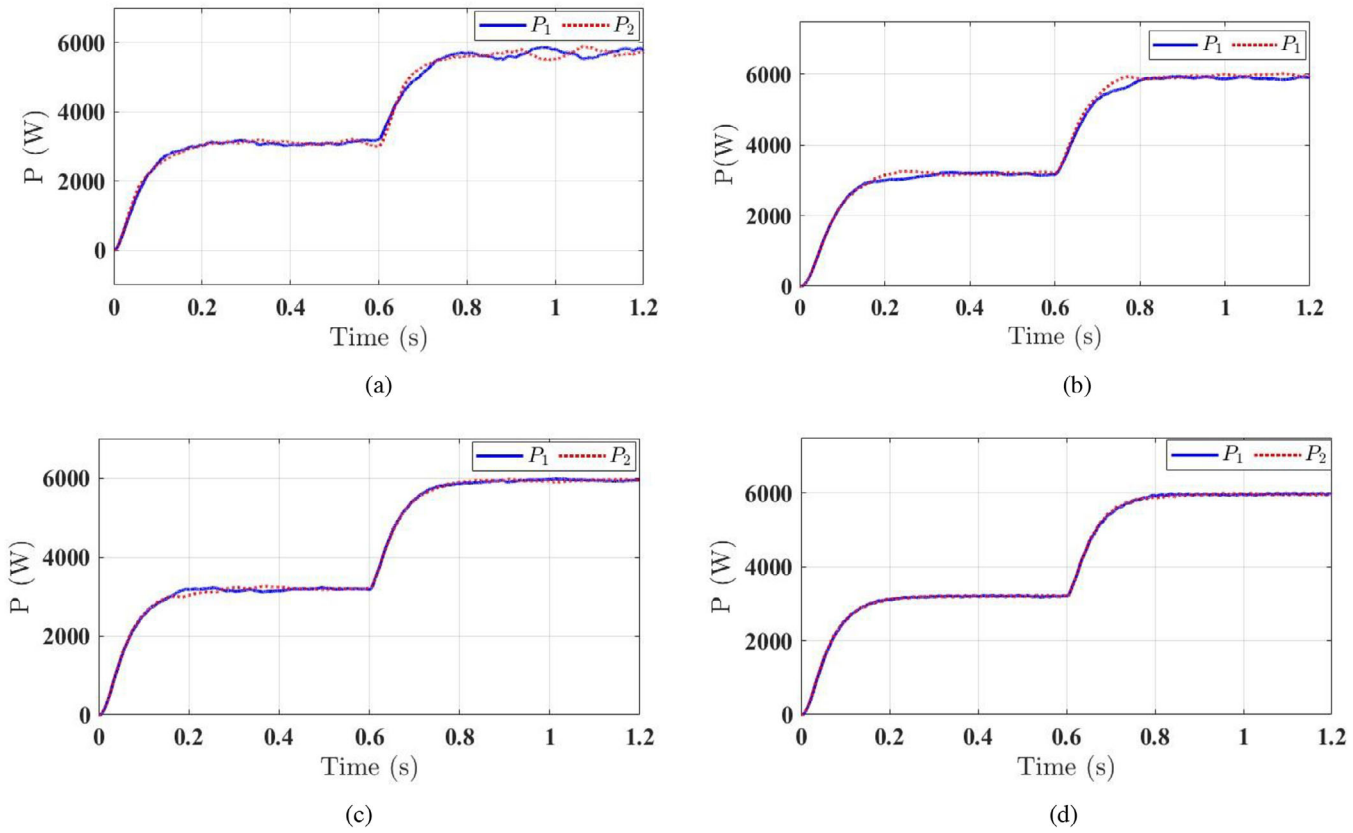

FIGURE 6 Active power-sharing using different controllers: (a) PID, (b) Equation (12), (c) Equation (13), and (d) Equation (14).

4.1 | Simulation analysis

Figure 4 illustrates the frequency response of both DGs using different controllers. In Figure 4a, the application of a PID controller for voltage and current controller loops results in a system that takes a long time to recover its frequency. The introduction of a second load at time $t = 0.6$ s causes the frequency to decrease, leading to a longer stabilization time.

In Figure 4b, the frequency response for a system utilizing a sliding surface described by Equation (12) shows a slower stabilization time compared to the PID controller, with some ripples in the system after the second load is added. Figure 4c, on the other hand, utilizes Equation (13) in the system, resulting in a quicker stabilization time. When the second load is introduced, the frequency of the DGs remains smooth and consistent.

To further enhance the stability of the system, an integral term is added to Equation (13) to define the slide surface as in (14), as shown in Figure 4d. This modification helps to remove the ripples from the system and improves its overall stability.

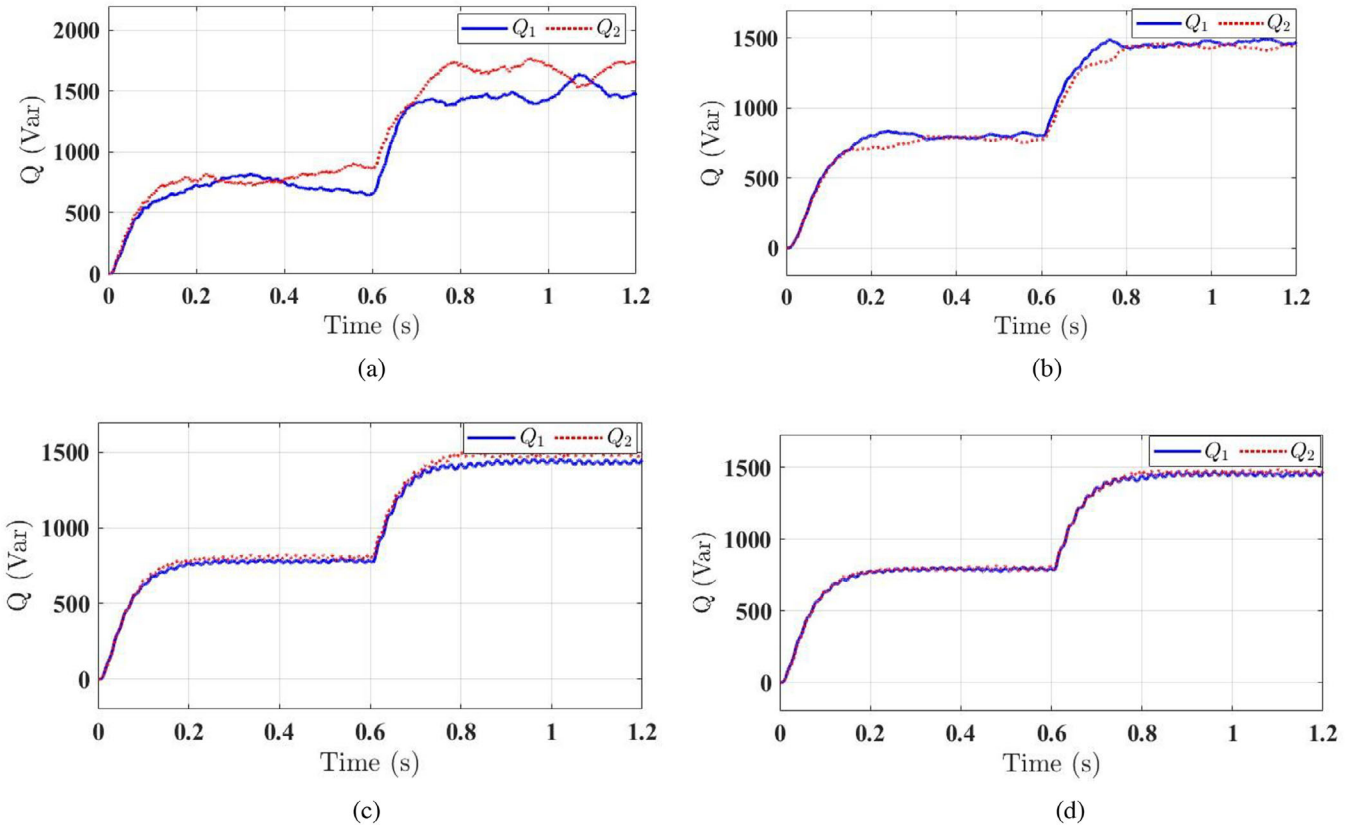

FIGURE 7 Active power-sharing using different controllers: (a) PID, (b) Equation (12), (c) Equation (13), and (d) Equation (14).

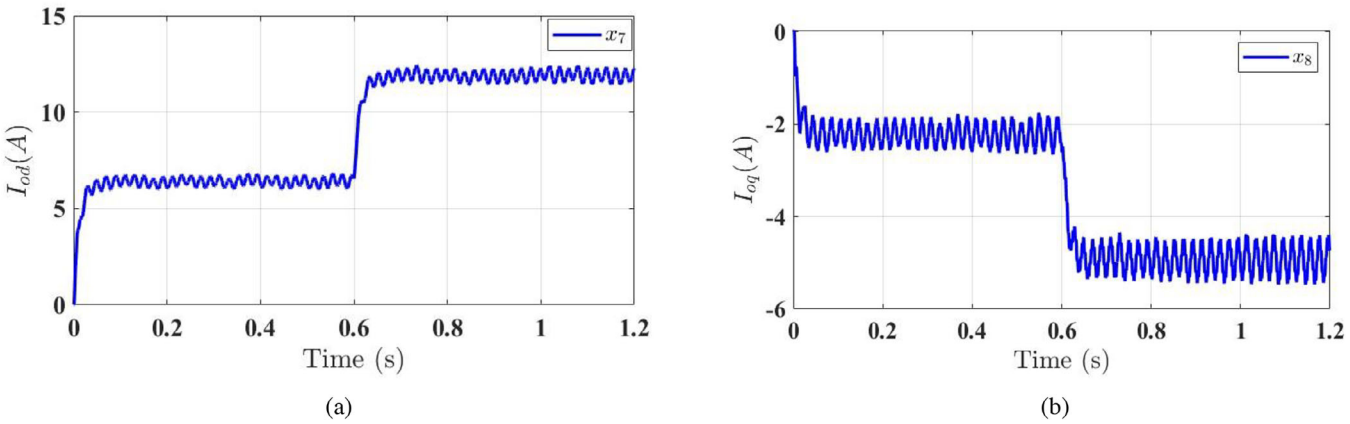

FIGURE 8 Zero dynamic system (a) direct output current, (b) quadrature output current.

Figure 5 illustrates how the system is affected by the switch gain. While a positive parameter is a step in the right direction, it must be sufficiently large to ensure system stability. As shown in Figure 5b, the direct output voltage drops to zero when k is not large enough, leading to frequency droop and system instability as depicted in Figure 5a.

The system's active power is calculated using the (*d*–*q*) output voltage and current. In Figure 6, different strategies for active power sharing are compared. Initially, the active power is equally divided between two DGs, with each DG providing 3000 W from t = 0–0.6 s. As a new load is added, the active power increases to 6000 W for each DG from t = 0.6–1.2 s. Analysis of Figure 6d shows that utilizing Equation (14) improves the accuracy in sharing active power.

Figure 7 illustrates the reactive power sharing within the system achieved through various controllers. It is evident that utilizing a PID controller results in unequal power-sharing with noticeable oscillations, particularly with DG1 often absorbing

an excessive amount of reactive power, causing inaccuracies. Conversely, employing sliding controller strategies offers more stability in reactive power distribution. The sliding surface Equation (14) significantly improves the smooth and accurate transient performance of reactive power sharing, as demonstrated in Figure 7d.

Figure 8 illustrates the stability of the zero-dynamic of the system as proven in the feedback linearization section. Specifically, Figure 8a demonstrates the stability of the direct output current, while Figure 8b represents the quadrature output current denoted as x_7, and x_8 in the dynamic system, respectively. The active and reactive power states, x_1, and x_2, correspond to Figures 6 and 7, respectively.

5 | CONCLUSION

Here, a new strategy called fraction order sliding control was proposed to control the primary controller of an isolated microgrid with two DGs connected to some fluctuating loads. Then, the dynamic equations of the system were written in the $d-q$ frame, which became a non-linear MIMO system. V_d and V_q were proposed as outputs. Moreover, input/output feedback linearization is used to transform the non-linear equations into linear equations and FOSMC is inserted into the resulting system. FOSMC was designed using the Lyapunov stability method. The designed controller has been proven and shown to be stable and can adjust the frequency and voltage of the microgrid, and ensure a balanced distribution of power between the two DG systems. The result of the simulation demonstrated that the strategy has a more stabilizing effect on the microgrid system since the FOSMC provides more turning parameters compared to traditional and simple fractional derivative sliding mode controllers that are used to improve stability and robustness.

AUTHOR CONTRIBUTIONS

Mohamad Issa Ibraheem: Conceptualization; data curation; resources; software; writing—original draft. **Mehdi Edrisi**: Conceptualization; investigation; methodology; supervision; writing—review and editing. **Hassan Haes Alhelou**: Conceptualization; methodology; supervision; writing—review and editing. **Mehdi Gholipour**: Conceptualization; resources; supervision; writing—review and editing.

CONFLICT OF INTEREST STATEMENT

The authors declare no conflicts of interest.

DATA AVAILABILITY STATEMENT

The data that support the findings of this study are available from the corresponding author upon reasonable request.

ORCID

Hassan Haes Alhelou https://orcid.org/0000-0001-8176-1589
Mehdi Gholipour https://orcid.org/0000-0001-7176-935X

REFERENCES

1. Saeed, M.H., Fangzong, W., Kalwar, B.A., Iqbal, S.: A review on microgrids' challenges perspectives. IEEE Access 9, 166502–166517 (2021). https://doi.org/10.1109/ACCESS.2021.3135083
2. Fathi, A., Shafiee, Q., Bevrani, H.: Robust frequency control of microgrids using an extended virtual synchronous generator. IEEE Trans. Power Syst. 33(6), 6289–6297 (2018). https://doi.org/10.1109/TPWRS.2018.2850880
3. Wali, S.B., et al.: Battery storage systems integrated renewable energy sources: A biblio metric analysis towards future directions. J. Energy Storage 35, 102296 (2021). https://doi.org/10.1016/j.est.2021.102296
4. Motjoadi, V., Bokoro, P.N., Onibonoje, M.O.: A review of microgrid-based approach to rural electrification in South Africa: Architecture and policy framework. Energies 13(9), 1–22 (2020). https://doi.org/10.3390/en13092193
5. Mohamed, Y.A-R.I., Radwan, A.A.: Hierarchical control system for robust microgrid operation and seamless mode transfer in active distribution systems. IEEE Trans. Smart Grid 2(2), 352–362 (2011). https://doi.org/10.1109/TSG.2011.2136362
6. Bidram, A., Nasirian, V., Davoudi, A., Lewis, F.L.: Cooperative Synchronization in Distributed Microgrid Control, vol. 2017. Springer, Berlin (2017)
7. Rokrok, E., Shafie-khah, M., Catalão, J.P.S.: Review of primary voltage and frequency control methods for inverter-based islanded microgrids with distributed generation. Renewable Sustainable Energy Rev. 82, 3225–3235 (2017). https://doi.org/10.1016/j.rser.2017.10.022
8. Shanxu, D., Yu, M., Jian, X., Yong, K., Jian, C.: Parallel operation control technique of voltage source inverters in UPS. In: IEEE 1999 International Conference on Power Electronics and Drive Systems, PEDS'99, Hong Kong (1999). https://doi.org/10.1109/PEDS.1999.792823
9. Caldognetto, T., Tenti, P.: Microgrids operation based on master&slave cooperative control. IEEE J. Emerging Sel. Top. Power Electron. 2(4), 1081–1088 (2013). https://doi.org/10.1109/JESTPE.2014.2345052
10. Prodanović, M., Green, T.C.: High-quality power generation through distributed control of a power park microgrid. IEEE Trans. Ind. Electron. 53(5), 1471–1482 (2006). https://doi.org/10.1109/TIE.2006.882019
11. Majumder, R., Member, S., Ghosh, A.: Angle droop versus frequency droop in a voltage source converter based autonomous microgrid
12. Majumder, R., Chaudhuri, B., Ghosh, A., Majumder, R., Ledwich, G., Zare, F.: Improvement of stability and load sharing in an autonomous microgrid using supplementary droop control loop. IEEE Trans. Power Syst. 25(2), 796–808 (2010). https://doi.org/10.1109/TPWRS.2009.2032049
13. Rodriguez, P., Candela, I., Citro, C., Rocabert, J., Luna, A.: Control of grid-connected power converters based on a virtual admittance control loop. In: 15th European Conference on Power Electronics and Applications, pp. 1–10. Lille, France (2013). https://doi.org/10.1109/EPE.2013.6634621
14. Rokrok, E., Mahmoudi, A.: A voltage/frequency control scheme for distributed resources in an autonomous multi-bus microgrid. In: 24th Iranian Conference on Electrical Engineering (ICEE), pp. 954–959. Shiraz, Iran (2016). https://doi.org/10.1109/IranianCEE.2016.7585659
15. Mohamed, Y.A.R.I., El-Saadany, E.F.: Adaptive decentralized droop controller to preserve power sharing stability of paralleled inverters in distributed generation microgrids. IEEE Trans. Power Electron. 23(6), 2806–2816 (2008). https://doi.org/10.1109/TPEL.2008.2005100
16. Rokrok, E., Golshan, M.E.H.: Adaptive voltage droop scheme for voltage source converters in an islanded multibus microgrid. IET Gener. Transm. Distrib. 4(5), 562 (2010). https://doi.org/10.1049/iet-gtd.2009.0146
17. Mohammadi, J., Ajaei, F.B.: Improved mode-adaptive droop control strategy for the DC microgrid. IEEE Access 7, 86421–86435 (2019). https://doi.org/10.1109/ACCESS.2019.2924994
18. Tah, A., Das, D.: An enhanced droop control method for accurate load sharing and voltage improvement of isolated and interconnected DC microgrids. IEEE Trans. Sustainable Energy 7(3), 1194–1204 (2016). https://doi.org/10.1109/TSTE.2016.2535264
19. Dheer, D.K., Gupta, Y., Doolla, S.: A self adjusting droop control strategy to improve reactive power sharing in islanded microgrid. IEEE Trans. Sustainable Energy 11, 1624–1635 (2019). https://doi.org/10.1109/TSTE.2019.2933144

20. Zhang, L., Zheng, H., Hu, Q., Su, B., Lyu, L.: An adaptive droop control strategy for islanded microgrid based on improved particle swarm optimization. IEEE Access 8, 3579–3593 (2020). https://doi.org/10.1109/ACCESS.2019.2960871
21. Unnikrishnan, B.K., Johnson, M.S., Cheriyan, E.P.: Small signal stability improvement of a microgrid by the optimised dynamic droop control method. IET Inst. Eng. Technol. 14, 822–833 (2020). https://doi.org/10.1049/iet-rpg.2019.0428
22. Yuan, W., Wang, Y., Liu, D., Deng, F., Chen, Z.: Efficiency-prioritized droop control strategy of AC microgrid. IEEE J. Emerging Sel. Top. Power Electron. 9, 2936–2950 (2020). https://doi.org/10.1109/JESTPE.2020.2967756
23. Keyvani, B., Fani, B., Karimi, H., Moazzami, M., Shahgholian, G.: Improved droop control method for reactive power sharing in autonomous. J. Renewable Energy Environ. 9(3), 1–9 (2022). https://doi.org/10.30501/jree.2021.298138.12351
24. Kulkarni, S.V., Gaonkar, D.N.: Improved droop control strategy for parallel connected power electronic converter based distributed generation sources in an Islanded Microgrid. Electr. Power Syst. Res. 201, 107531 (2021). https://doi.org/10.1016/j.epsr.2021.107531
25. Shabbir, M.N.S.K., Liang, X., Li, W., Imtiaz, S., Quaicoe, J.: A model predictive control-based voltage and frequency regulation through distributed generation in isolated microgrids: Part I development and parameterization of the data-driven predictive model. In: IEEE/IAS 58th Industrial and Commercial Power Systems Technical Conference. Las Vegas, NV, USA (2022). https://doi.org/10.1109/ICPS54075.2022.9773940
26. Dashtdar, M., et al.: Improving the power quality of island microgrid with voltage and frequency control based on a hybrid genetic algorithm and PSO. IEEE Access 10, 105352–105365 (2022). https://doi.org/10.1109/ACCESS.2022.3201819
27. Andrade, F.: New model of a converter-based generator using electrostatic synchronous machine concept. IEEE Trans. Energy Convers. 29(2), 344–353 (2014). https://doi.org/10.1109/TEC.2014.2303827
28. Bidram, A., Member, S., Davoudi, A., Lewis, F.L., Guerrero, J.M., Member, S.: Distributed cooperative secondary control of microgrids using feedback linearization. IEEE Trans. Power Syst. 28(3), 3462–3470 (2013)
29. Dou, C., Zhang, Z., Yue, D., Song, M.: Improved droop control based on virtual impedance and virtual power source in low-voltage microgrid. IET Gener. Transm. Distrib. 11(4), 1046–1054 (2016). https://doi.org/10.1049/iet-gtd.2016.1492
30. Josep, M., Juan, V., Guerrero, J.M., Vásquez, J.C., Teodorescu, R.: Hierarchical control of droop-controlled DC and AC microgrids – A general approach towards standardization. IEEE Trans. Ind. Electron. 58(1), 158–172 (2011). https://doi.org/10.1109/TIE.2010.2066534
31. Slotine, J.-J.E., Li, W.: Applied Nonlinear Control. Prentice-Hall, Saddle River, NJ (1991)
32. Lu, Q., Sun, Y., Mei, S.: Nonlinear control systems and power system dynamics. Kluwer Academic Publishers (2001)
33. Fernandez, B., Hedrick, J.K.: Control of multivariable non-linear systems by the sliding mode method. Int. J. Control 46, 1019–1040 (1987). https://doi.org/10.1080/00207178708547410
34. Zhang, D., Cao, L., Tang, S.: Fractional-order sliding mode control for a class of uncertain nonlinear systems based on LQR. Int. J. Adv. Robot. Syst. 14(2) (2017)

How to cite this article: Ibraheem, M.I., Edrisi, M., Alhelou, H.H., Gholipour, M.: Fractional order slide mode droop control for simultaneous voltage and frequency regulation of AC microgrid. IET Renew. Power Gener. 18, 2629–2640 (2024). https://doi.org/10.1049/rpg2.13067